Mechanism and Machine Theory 144 (2020) 103647

Contents lists available at ScienceDirect

Mechanism and Machine Theory

journal homepage: www.elsevier.com/locate/mechmachtheory

Research paper

Motorcycle final drive geometry optimization on uneven roads

M. Alcazar[a,*], J. Perez[a], J.E. Mata[b], J.A. Cabrera[a], J.J. Castillo[a]

[a] Department of Mechanical Engineering, University of Málaga, Málaga 29071, Spain
[b] Department of Mechanical and Mining Engineering, University of Jaén, Jaén 23071, Spain

ARTICLE INFO

Article history:
Received 25 July 2019
Revised 19 September 2019
Accepted 30 September 2019

Keywords:
Motorcycle modeling
Final drive
Genetic algorithm optimization
Transient tire model

ABSTRACT

The design of transmission systems plays an important role in the dynamic performance of motorcycles. It is well known that power delivery and stability in motorcycles is strongly affected by the geometry of the final drive.

This article presents a 2D multibody motorcycle model in which the tire and final drive are considered thoroughly. A nonlinear transient model is used to reproduce forces between the tire and the road. The engine and wheel sprockets, the squat ratio and the chain slack have been taken into account in the final drive kinematic model.

The configuration of the final drive elements and its influence on the distance covered by the motorcycle have been studied. Furthermore, the motorcycle final drive design has been optimized to maximize the distance traveled on different uneven roads.

Simulations show a superior performance of the motorcycle when the configuration of the final drive elements is optimized. This study contributes to demonstrating the importance of the configuration and geometry of the final drive to improve stability and overall behavior of the motorcycle on uneven roads.

1. Introduction

It is well known that the motorcycle final drive design plays an important role in engine-to-slip dynamics. There are at least four parameters involved in this phenomenon [1], namely:

1. Longitudinal velocity
2. Tire radial compliance
3. Swingarm motion
4. Slip due to wheel rotation

Nowadays, different final drive technologies coexist. The most important ones are continuously variable transmission (CVT) [2], cardan shaft, V-belt and roller chain [3]. The study of this system is of great importance in the analysis of power transmission and motorcycle stability. Besides, the dynamics of this system are also of great importance in the design of TCS and ABS. For example, in [4,5] the resonance phenomena associated with variations in the longitudinal force in the rear wheel and their influence on the stability of the motorcycle are studied. A study of the final drive is carried out in [6]. The

* Corresponding author.
E-mail addresses: manuel.alcazar@uma.es (M. Alcazar), javierperez@uma.es (J. Perez), jemata@ujaen.es (J.E. Mata), jcabrera@uma.es (J.A. Cabrera), juancas@uma.es (J.J. Castillo).

https://doi.org/10.1016/j.mechmachtheory.2019.103647
0094-114X/

Nomenclature

Symbol	Magnitude
x	x-coordinate
y	y-coordinate
a	Angular design parameter
L	Longitudinal design parameter
H_y	Height of the ground
λ	Wavelength of the ground
σ	Width of the bump
μ	x-coordinate of the center of the bump
α	Angular coordinate of the engine sprocket
β	Angular coordinate of the wheel sprocket
γ	Upper chain angle
k	Stiffness coefficient
c	Damping coefficient
s	Unloaded length
$\mathbf{\Phi}$	Kinematic set of equations
$\mathbf{q}$	Coordinate vector
$\dot{\mathbf{q}}$	Velocities vector
$\ddot{\mathbf{q}}$	Accelerations vector
SR	Squat ratio
d	Distance traveled

kinematic relationships of the final drive and the dynamic behavior of the front and rear suspension are studied by varying the vertical position of the engine sprocket. Finally, an analysis of power transmission in motorcycles is carried out in [7]. In this work, three models consider the stiffness of the tire and the final drive is described.

The modeling of in-plane dynamics is required to analyze the acceleration process of a motorcycle. To the best of our knowledge, there are basically two complete motorcycle models described in literature. The first one was published by Sharp in 2001. It makes use of independent coordinates to study motorcycle dynamics [8]. This model, with slight modifications, is currently used by the BikeSim commercial simulation package. The second model was published by Cossalter and Lot in 2002. In this case, natural coordinates are used to reproduce the dynamics of the motorcycle [9]. The FastBike commercial simulation package is based on this model.

Furthermore, the tire model is of great importance in the modeling of the motorcycle. There are several contact force models, such as: the restitution coefficient [10], spring-shock absorber systems and the Hertz contact theory [11], among others. Besides, there are also several friction force models [12], for example: Coulomb, Stribeck, Threlfall and LuGre, among others. The most widely used formulation for modeling tire-road friction was established by Pacejka, using the well-known «magic formula» [13]. This model describes both stationary and transient tire behavior. Transient behavior is modeled using a parameter known as relaxation length. Other authors, although they resort to Pacejka's stationary model, propose an alternative transient model. In this approach, they consider the stiffness of the tire instead of a relaxation length [9]. This model allows the slip and contact force to be delayed, modeling the relationship between them by means of a first-order system. Both Pacejka's transient model [13] as well as Cossalter's model [9] are equivalent, as shown in [7], the latter having a more physical sense than the former.

Four-wheeled vehicles have received great attention from research groups. However, research studies focused on two-wheeled vehicles are less common. Although lateral relaxation lengths for various motorcycle tires have been published in literature [14], no studies related to longitudinal relaxation lengths have been found.

The modeling of the final drive can be performed from several perspectives and with different simplifications. The relationships between the engine sprocket, wheel and swingarm can be modeled using kinematic constraints [7,15], dynamical constraints [6] or a combination of both [7]. Dynamic models consider chain stiffness and damping as well as the elastic coupling that exists between the sprocket and the rim. However, these parameters are difficult to measure. Furthermore, incorrect estimates affect the performance and accuracy of the simulations. In this work, these relationships are kinematic, which makes the modeling process less complex and computationally more efficient.

This paper proposes a methodology for the optimal design of motorcycle final drives by means of multibody simulation and genetic algorithms. As found in [16,17], genetic algorithms are an extensively used tool to optimize multiple physical processes, offering an optimal solution in complex multi-variable systems.

In this work, an in-plane motorcycle model with the following features is proposed:

- The final drive has been modeled in detail, analyzing the kinematic relationships between the wheel, the swingarm and the engine sprocket.

- The road-tire contact has been modeled using the Pacejka transient model [13], considering a constant tire relaxation length. The variable effective radius is modeled by considering the radial deformation of the tire.
- Three different road profiles have been simulated: flat, bumpy and sinusoidal.
- Aerodynamics have not been considered.
- The dynamic problem has been formulated by using the augmented Lagrangian formulation [18].
- Multi-step integrators (Adams-Bashforth and Adams-Moulton) have been used [19].
- The modeling of the system has been carried out by means of natural coordinates [18,20].

Real time performance has been achieved thanks to dynamic formulation and the solver used. In addition, due to the tire model considered, the simulation can start from a singularity, such as standstill as well as moving forwards or backwards.

Once the model simulations have been carried out, the parameters that influence the behavior of the motorcycle on an uneven road are studied. These parameters have been optimized by means of genetic algorithms, obtaining the final drive design that maximizes the distance traveled in the test.

This work is organized as follows: in Section 2 the model of the motorcycle is described, including the coordinates and constraints used. Section 3 is devoted to the description of the numerical algorithm employed, both for the formulation of the Differential-Algebraic set of Equations (DAE) and for its solution. In Section 4, the optimization of the problem under consideration is performed, which is the maximization of the distance traveled by the motorcycle. The results obtained are shown and commented in Section 5. Finally, in Section 6, the conclusions of the work are presented.

2. System definition and modeling

2.1. Motorcycle description

In this paper, the motorcycle has been modeled as a system composed of six bodies: chassis, swingarm, engine sprocket, lower front suspension, rear wheel and front wheel. Both the rider and the upper part of the front suspension are assumed to be rigidly attached to the chassis. This simplification has been made because only the in-plane dynamics of the motorbike are studied. A fork and a spring-shock absorber are used in the front and rear suspension respectively. The coordinate system used is the following: horizontal x axis increasing to the right while the y axis is vertical, increasing to the top. The number of degrees of freedom (DoF) of the system is 6 (Fig. 1). These DoF are associated with the bounce (1) and longitudinal translation (2) of the motorcycle chassis, the pitch (3), the rotation of the rear wheel and engine sprocket (4) and the rear and front hop (5 and 6). The rotation of the front wheel is not considered due to the computational cost of solving the tire-road interaction twice. Thus, the convergence of the simulation has been increased as only a pure traction scenario is considered. Neither aerodynamic forces nor rolling resistance have been considered in order to be able to analyse the phenomena under study independently.

A total of 39 coordinates are used to model the motorcycle (Table 1). 30 natural coordinates describe the movement of the 15 points shown in Fig. 3. The remaining 9 coordinates are grouped into two types: lengths associated with the four damper-spring systems considered and five angles. Three angles are associated with the transmission and the other two with the pitch of the chassis and swingarm.

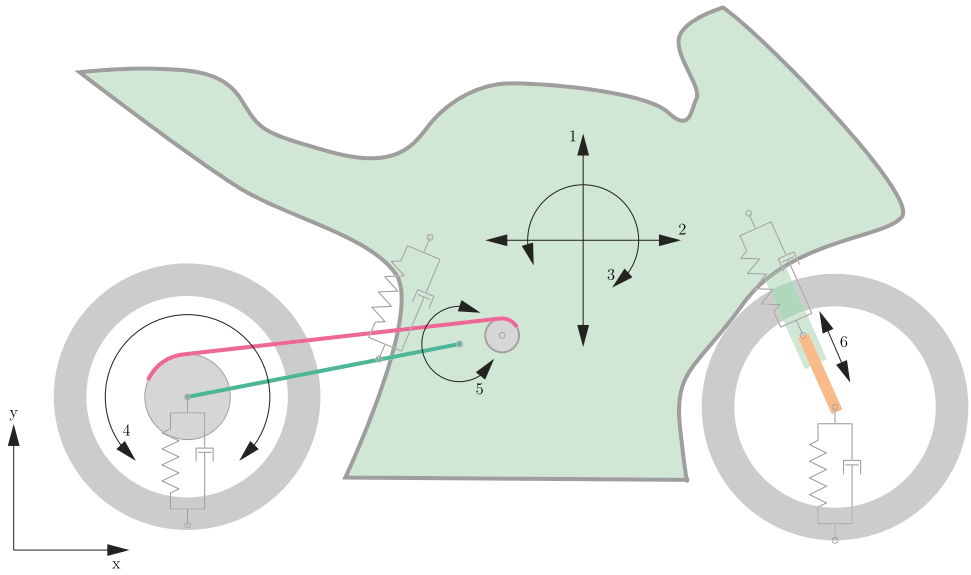

Fig. 1. Dynamic model of the motorcycle.

Table 1
Coordinates.

Coordinate	Description	Coordinate	Description
x_1	Swingarm axis	x_{11}	Wheel sprocket tangential point
y_1		y_{11}	
x_2	Engine axis	x_{12}	Upper point fork suspension
y_2		y_{12}	
x_3	Upper damper pin	x_{13}	Front wheel axis
y_3		y_{13}	
x_4	Upper triple clamp	x_{14}	Rear tire contact point
y_4		y_{14}	
x_5	Lower triple clamp	x_{15}	Front tire contact point
y_5		y_{15}	
x_6	Rear wheel axis	rs	Rear suspension length
y_6		fs	Front suspension length
x_7	Lower damper pin	rt	Rear tire radii
y_7		ft	Front tire radii
x_8	Engine reference point	θ	Chassis angle
y_8		α	Engine sprocket angle
x_9	Rear wheel reference point	β	Wheel sprocket angle
y_9		γ	Upper chain angle + $\pi/2$
x_{10}	Engine sprocket tangential point	ϕ	Swingarm angle
y_{10}			

Table 2
Inertial properties of each body.

Body No.	Ref.	m [kg]	I_{CoG} [kg m^2]
I	Chassis + rider	223.0	26.20
II	Swingarm	10.0	0.80
III	Engine sprocket	1.0	0.50
IV	Rear wheel	16.2	0.66
V	Lower part front fork	7.0	0.18
VI	Front wheel	12.0	0.47

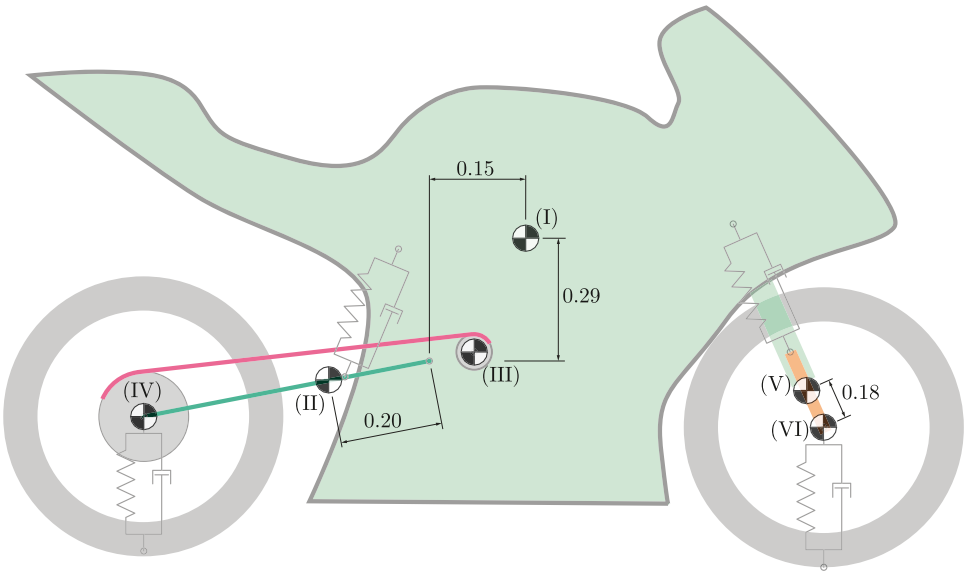

Fig. 2. Locations of the centers of mass of the motorcycle bodies.

The masses and moments of inertia of the bodies that constitute the system have been extracted from [9,21]. They are shown in Table 2 and Fig. 2. The geometry of the motorcycle as well as the parameters of the spring-shock absorber systems which have been obtained from [9,21] are shown in Table 3.

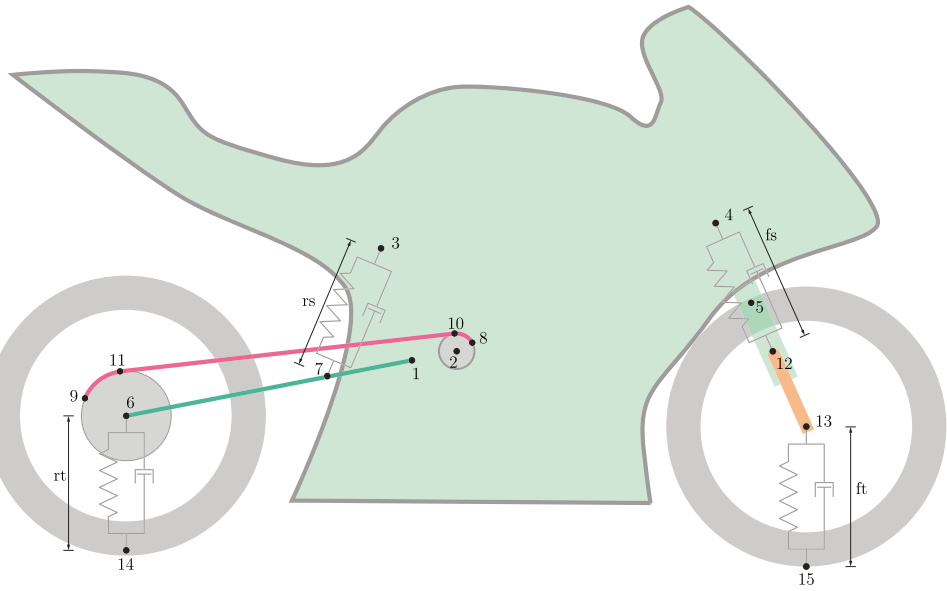

Fig. 3. Motorcycle coordinates.

Table 3
The most important parameters of the motorcycle.

Parameter	Value	Units
Rear equivalent stiffness	19,900	N/m
Rear equivalent damping coef.	3960	Ns/m
Rear unsprung mass	24.5	kg
Front equivalent stiffness	20,800	N/m
Front equivalent damping coef.	1750	Ns/m
Front unsprung mass	19.9	kg
Rear weight distribution	50.7	%
Front weight distribution	49.3	%
Center of gravity height	623	mm
Total mass	272	kg
Wheelbase	1424	mm
Caster angle	24	deg

2.2. Kinematics

Kinematic constraints are grouped into three blocks, namely: motorcycle, transmission and tire-road contact (road profile).

2.2.1. Kinematic model of the motorcycle

The «kinematic model of the motorcycle» refers to the set of equations that governs the kinematics of the chassis, rear axle, front axle and wheels. The kinematic relationships that model transmission as well as tire-road interaction are described in an independent Section.

Five points are used to model the chassis. Points 1 and 2 represent the axle of the swingarm and engine sprocket respectively. Point 3 is the upper anchorage of the rear shock absorber. Points 4 and 5 are used to define the front suspension slider. In addition, the lengths and angles listed in Table 4 are also defined. Eqs. (1)–(8) are the kinematic constraints of the chassis.

$$x_1 + L_2 \cos(\theta + a_2) - x_2 = 0 \tag{1}$$

$$y_1 + L_2 \sin(\theta + a_2) - y_2 = 0 \tag{2}$$

$$x_1 + L_3 \cos(\theta + a_3) - x_3 = 0 \tag{3}$$

$$y_1 + L_3 \sin(\theta + a_3) - y_3 = 0 \tag{4}$$

Table 4
Motorcycle design parameters.

Design Parameter	Description	Value	Units
L_2	$\|\|\mathbf{r}_{1\to 2}\|\|$	variable	m
L_3	$\|\|\mathbf{r}_{1\to 3}\|\|$	0.260	m
L_4	$\|\|\mathbf{r}_{1\to 4}\|\|$	0.767	m
L_5	$\|\|\mathbf{r}_{1\to 5}\|\|$	0.786	m
a_2	$\measuredangle\mathbf{r}_{1\to 2}$	variable	rad
a_3	$\measuredangle\mathbf{r}_{1\to 3}$	1.850	rad
a_4	$\measuredangle\mathbf{r}_{1\to 4}$	0.785	rad
a_5	$\measuredangle\mathbf{r}_{1\to 5}$	0.000	rad
L_7	$\|\|\mathbf{r}_{1\to 7}\|\|$	0.200	m
L_{SA}	$\|\|\mathbf{r}_{1\to 6}\|\|$	0.560	m
θ_0	Chassis pitch angle	0.000	rad
φ_0	Swingarm angle	3.316	rad
rt_0	Unloaded rear tire radius	0.300	m
ft_0	Unloaded front tire radius	0.300	m
R_{WS}	Wheel sprocket radius	variable	m
R_{ES}	Engine sprocket radius	variable	m
L	Fixed chain length	variable	m
H_y	Height of ground irregularities	variable	m
μ	Bump center x-coordinate	variable	m
λ	Wavelength of ground irregularities	variable	m
σ	Bump width	variable	m
L_8	$\|\|\mathbf{r}_{12\to 13}\|\|$	0.350	m

$$x_1 + L_4 \ \cos(\theta + a_4) - x_4 = 0 \tag{5}$$

$$y_1 + L_4 \ \sin(\theta + a_4) - y_4 = 0 \tag{6}$$

$$x_1 + L_5 \ \cos(\theta + a_5) - x_5 = 0 \tag{7}$$

$$y_1 + L_5 \ \sin(\theta + a_5) - y_5 = 0 \tag{8}$$

The rear train kinematics are defined by points 6 and 7. The first point is the rear wheel axis and the second one is the lower anchorage of the shock absorber. It is important to note that φ is the angle that forms the swingarm with the horizontal and not with the chassis. The length of the rear shock-absorber is determined by coordinate *rs*.

$$x_1 + L_{SA} \ \cos\varphi - x_6 = 0 \tag{9}$$

$$y_1 + L_{SA} \ \sin\varphi - y_6 = 0 \tag{10}$$

$$x_1 + L_7 \ \cos\varphi - x_7 = 0 \tag{11}$$

$$y_1 + L_7 \ \sin\varphi - y_7 = 0 \tag{12}$$

$$(x_3 - x_7)^2 + (y_3 - y_7)^2 - rs^2 = 0 \tag{13}$$

The kinematic constraints of the front fork suspension slider mechanism are defined by Eqs. (14)–(15). The length of the lower part of the front suspension is determined by parameter L_8. Coordinate *fs* is the front spring-shock absorber length.

The length of the lower part of the front suspension and the front spring-shock absorber is given by parameter L_8 and coordinate *fs*, respectively.

$$(x_5 - x_4)(y_{13} - y_{12}) - (y_5 - y_4)(x_{13} - x_{12}) = 0 \tag{14}$$

$$(x_5 - x_4)(y_{13} - y_4) - (y_5 - y_4)(x_{13} - x_4) = 0 \tag{15}$$

$$(x_{13} - x_{12})^2 + (y_{13} - y_{12})^2 - L_8^2 = 0 \tag{16}$$

$$(x_4 - x_{12})^2 + (y_4 - y_{12})^2 - fs^2 = 0 \tag{17}$$

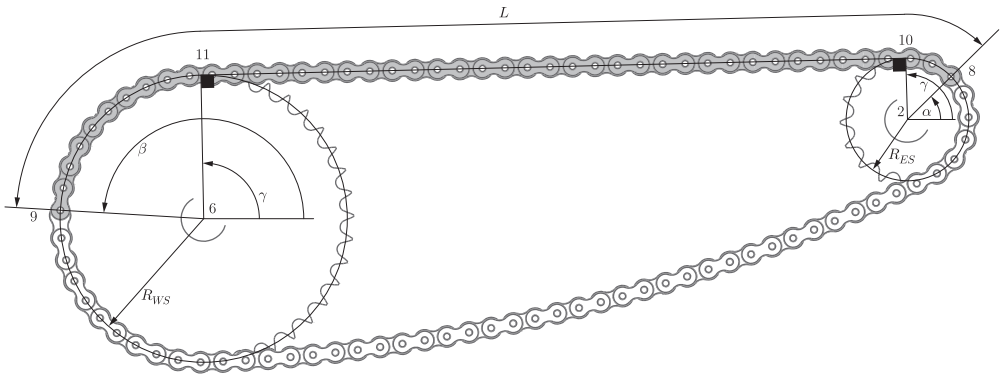

Fig. 4. Coordinates and parameters of transmission kinematics.

The wheel equations are (18)–(21):

$$x_6 - x_{14} = 0 \tag{18}$$

$$x_{13} - x_{15} = 0 \tag{19}$$

$$y_6 - y_{14} - rt = 0 \tag{20}$$

$$y_{13} - y_{15} - ft = 0 \tag{21}$$

2.2.2. Kinematic model of the transmission

Four points (8)–(11) and three additional angles (α, β, γ) are used to model transmission kinematics. The pitch radii of the engine and wheel sprockets are R_{ES} and R_{WS} respectively. Parameter L is the length of the section of the chain between points 8 and 9 (Fig. 4). This length is constant throughout the simulation. Neither the 'polygonal action' that takes place in chain transmissions [22,23] nor the efficiency of the transmission are modeled.

Eqs. (22)–(29) locate points 8 – 11 with respect to the sprocket's axes. Eq. (30) defines length L, while Eq. (31) determines the orthogonality condition of vectors $\mathbf{r}_{6\to 11}$ and $\mathbf{r}_{11\to 10}$.

$$x_2 + R_{ES}\ \cos\alpha - x_8 = 0 \tag{22}$$

$$y_2 + R_{ES}\ \sin\alpha - y_8 = 0 \tag{23}$$

$$x_2 + R_{ES}\ \cos\gamma - x_{10} = 0 \tag{24}$$

$$y_2 + R_{ES}\ \sin\gamma - y_{10} = 0 \tag{25}$$

$$x_6 + R_{WS}\ \cos\beta - x_9 = 0 \tag{26}$$

$$y_6 + R_{WS}\ \sin\beta - y_9 = 0 \tag{27}$$

$$x_6 + R_{WS}\ \cos\gamma - x_{11} = 0 \tag{28}$$

$$y_6 + R_{WS}\ \sin\gamma - y_{11} = 0 \tag{29}$$

$$(\gamma - \alpha)R_{ES} + \sqrt{(x_{10} - x_{11})^2 + (y_{10} - y_{11})^2} + (\beta - \gamma)R_{WS} - L = 0 \tag{30}$$

$$(x_6 - x_{11})(x_{11} - x_{10}) + (y_6 - y_{11})(y_{11} - y_{10}) = 0 \tag{31}$$

Fig. 5 is used to illustrate the kinematic relationship between the two sprockets. In this Figure, it can be seen how an angular movement appears in the wheel when the swingarm moves keeping the engine sprocket locked. This movement

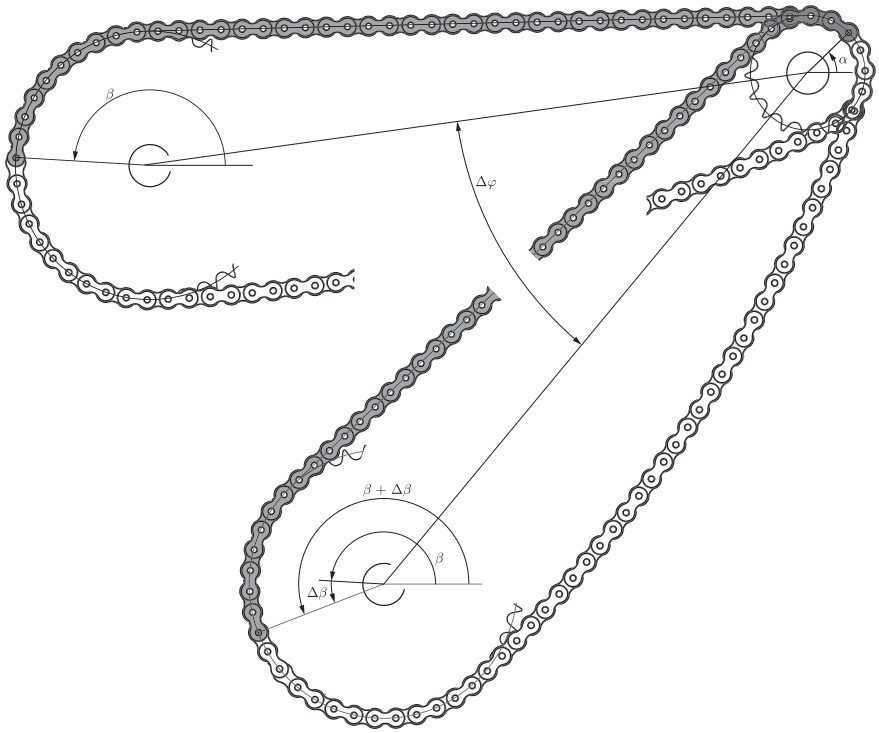

Fig. 5. Graphical demonstration of the movement induced in the wheel when the swingarm moves.

is common in a motorcycle riding on uneven roads. This way, the relationship between the angular speeds of the engine sprocket and the wheel are not determined only by the ratio between the number of teeth of the sprockets. Therefore, the previously described angular movement has to be taken into account to properly model the whole system. This statement is of great importance in the present work because it shows that, as angular accelerations appear in the drivetrain, power transmission from the engine to the wheel is strongly influenced by the design of the final drive.

2.2.3. Test surface profiles

Three different road profiles are simulated in this work, namely:

1. Sinusoidal profile
2. Gaussian profile (bumpy)
3. Flat profile

The coordinates of points 14 and 15 (Fig. 3) are given by equations (32) and (33) according to the type of road: sinusoidal, Gaussian and flat.

$$y_{14} - H_y \sin\left(\frac{2\pi}{\lambda} x_{14}\right) = 0 \tag{32a}$$

$$y_{14} - H_y \exp\left(-\frac{(x_{14} - \mu)^2}{2\sigma^2}\right) = 0 \tag{32b}$$

$$y_{14} = 0 \tag{32c}$$

$$y_{15} - H_y \sin\left(\frac{2\pi}{\lambda} x_{15}\right) = 0 \tag{33a}$$

$$y_{15} - H_y \exp\left(-\frac{(x_{15} - \mu)^2}{2\sigma^2}\right) = 0 \tag{33b}$$

$$y_{15} = 0 \tag{33c}$$

Table 5
Parameters of spring-shock absorber systems.

No.	Suspension parameter	Description	Initial Value	Units
1	k_{rs}	Rear suspension stiffness	251,400	N/m
2	c_{rs}	Rear suspension damping coefficient	50,000	Ns/m
3	s_{rs}	Unloaded rear suspension length	0.327	m
4	k_{fs}	Front suspension stiffness	25,000	N/m
5	c_{fs}	Front suspension damping coefficient	2100	Ns/m
6	s_{fs}	Unloaded front suspension length	0.395	m
7	k_{rt}	Rear tire stiffness	141,000	N/m
8	c_{rt}	Rear tire damping coefficient	50	Ns/m
9	s_{rt}	Unloaded rear tire length	0.300	m
10	k_{ft}	Front tire stiffness	130,000	N/m
11	c_{ft}	Front tire damping coefficient	50	Ns/m
12	s_{ft}	Unloaded front tire length	0.300	m

2.3. Dynamics

The forces that govern the dynamics of the system are grouped into three distinct blocks: front and rear suspensions, vertical forces on the front and rear tires and longitudinal forces on the rear tire. The parameters of the spring-shock absorber systems for both suspensions and tires can be found in Table 5:

The front and rear suspension parameters have been selected so that the equivalent stiffness and damping coefficients on the wheels are similar to those used in [24].

2.3.1. Dynamic model of the suspensions

For the suspensions, it has been decided to use a linear model for both the spring and shock absorber. The equations that reproduce front and rear suspension forces are the following:

$$F_{fs} = -k_{fs}(fs - s_{fs}) - c_{fs}\dot{fs} \tag{34}$$

$$F_{rs} = -k_{rs}(rs - s_{rs}) - c_{rs}\dot{rs} \tag{35}$$

2.3.2. Vertical dynamics of the tires

The following model of a spring-shock absorber has been considered (36),(37). In this model, the vertical force is zero when there is no contact between the tire and the road:

$$F_{rt} = \begin{cases} -k_{rt}(rt - rt_0) - c_{rt}\ \dot{rt} & \text{if } rt < rt_0 \\ 0 & \text{if } rt \geq rt_0 \end{cases} \tag{36}$$

$$F_{ft} = \begin{cases} -k_{ft}(ft - ft_0) - c_{ft}\ \dot{rt} & \text{if } ft < ft_0 \\ 0 & \text{if } ft \geq ft_0 \end{cases} \tag{37}$$

2.3.3. Longitudinal dynamics of the tires

The *Magic-formula* «fully nonlinear transient model» [13] is used to model the longitudinal force. This model, despite its computational cost, is considered to be the most suitable one for this work. The reasons are the following:

- There are fluctuations in the vertical loads due mainly to road surface irregularities and the load transfer that takes place in acceleration processes of motorcycles.
- In pure acceleration processes, due to the power-to-weight ratio of motorcycles, the longitudinal acceleration is important and, consequently, the slip is also high.
- There are important angular accelerations in the powertrain due to the geometry of the transmission system. This causes high slip fluctuations, which makes the slip oscillate from the stable to the unstable zone of the longitudinal force curve.

It is important to define both the effective rolling radius, R_e, and the linear velocity, V_x. The effective rolling radius is defined in [25] and is given by Eq. (38):

$$R_e = \frac{2}{3}rt_0 + \frac{1}{3}rt \tag{38}$$

The speed of the rear wheel axle, V_x, has to be taken into account to calculate the real wheel slip. The difference between considering the speed of the wheel axle or the speed of the chassis is important, as demonstrated further ahead.

$$V_x = \dot{x}_6 \tag{39}$$

Finally, the longitudinal slip speed, V_{sx}, is defined in [13] according to expression (40), in which $\omega = -\dot{\beta}$ due to the sign criteria used:

$$V_{sx} = V_x - R_e\omega \tag{40}$$

Due to the reasons stated before, it is required to resort to the fully nonlinear transient model to properly reproduce tire-road interaction. This model (Eqs. (41)–(52)) is developed in [13]. In this model, a first-order differential equation has to be solved (42). In addition, at very low velocities ($|V_x| \leq V_{\text{low}}$) it is necessary to introduce an additional parameter ($k_{\text{v,low}}$) to ensure the convergence of the method.

$$\sigma_k^* = \max\left(\frac{\sigma_{\kappa 0}}{K_{x\kappa}} \cdot \frac{|F_x| + K_{x\kappa}\varepsilon_F}{|\kappa'| + \varepsilon_F}; \sigma_{\min}\right) \tag{41}$$

$$\frac{du}{dt} + \frac{1}{\sigma_k^*}|V_x|u = -V_{sx} \tag{42}$$

$$\kappa' = \frac{u}{\sigma_k^*} - \frac{\kappa_{V,low}}{K_{x\kappa}V_{sx}} \tag{43}$$

$$\kappa_{V,low} = \begin{cases} \frac{1}{2}\kappa_{V,low0}\left(1 + \cos\left(\pi\frac{|V_x|}{V_{low}}\right)\right) & \text{if } |V_x| \leq V_{low} \\ 0 & \text{if } |V_x| > V_{low} \end{cases} \tag{44}$$

$$F_x = D_x \sin\left(C_x \arctan\left(B_x\kappa' - E_x\left(B_x\kappa' - \arctan(B_x\kappa')\right)\right)\right) \tag{45}$$

$$C_x = p_{Cx1} \tag{46}$$

$$D_x = \mu_x F_z \tag{47}$$

$$\mu_x = p_{Dx1} + p_{Dx2}df_z \tag{48}$$

$$E_x = \left(p_{Ex1} + p_{Ex2}df_z + p_{Ex3}df_z^2\right) \cdot \left(1 - p_{Ex4}\,\text{sgn}(\kappa')\right) \tag{49}$$

$$K_{x\kappa} = F_z(p_{Kx1} + p_{Kx2}df_z) \cdot \exp\left(p_{Kx3}df_z\right) \tag{50}$$

$$B_x = K_{x\kappa}/(C_xD_x) \tag{51}$$

$$df_z = (F_z - F_{zo})/F_{zo} \tag{52}$$

The parameters related to the stationary Pacejka tire model have been extracted from [24], while the parameters related to the relaxation length (Table 7) have been obtained from [13]. Among the three tires available in literature (Table 6), the 160/70 rear tire is chosen in this paper.

Table 6
Magic formula pure longitudinal parameters of 120/70, 180/55 and 160/70 tires. [24].

	Front tire 120/70	Rear tire 180/55	Rear tire 160/70
p_{Cx1}	1.6064	1.6064	1.6064
p_{Dx1}	1.3806	1.3548	1.2017
p_{Dx2}	−0.041429	−0.060295	−0.092206
p_{Ex1}	0.0263	0.0263	0.0263
p_{Ex2}	0.27056	0.27056	0.27056
p_{Ex3}	−0.076882	−0.076882	−0.076882
p_{Ex4}	1.1268	1.1268	1.1268
p_{Kx1}	25,939	25,939	25,939
p_{Kx2}	−4.2327	−4.2327	−4.2327
p_{Kx3}	0.33686	0.33686	0.33686

Table 7
Relaxation length parameter values. [13].

Parameter	Description	Value	Units
$\kappa_{V,low0}$	Artificial damping parameter	770	Ns/m
$\sigma_{\kappa 0}$	Relaxation length at $\kappa' = 0$	0.2	m
σ_{min}	Minimum relaxation length	0.02	m
ϵ_F	Regularization parameter (Eq. (41))	0.01	–
V_{low}	Speed beyond which the additional damping disappears	2.5	m/s

3. Numerical algorithm

3.1. Kinematic-dynamic formulation: augmented Lagrangian

Lagrange equations in dependent coordinates [18] are given by expression (53):

$$\frac{d}{dt}\left(\frac{\partial T}{\partial \dot{\mathbf{q}}}\right) - \frac{\partial T}{\partial \mathbf{q}} + \mathbf{\Phi}_{\mathbf{q}}^{\mathbf{T}}\mathbf{\Phi}_{\mathbf{q}} = \mathbf{Q} \tag{53}$$

The kinetic energy, T, can be written as (54):

$$T = \frac{1}{2}\dot{\mathbf{q}}^{\mathbf{T}}\mathbf{M}\dot{\mathbf{q}} \tag{54}$$

The combination of expressions (53) and (54) yields the following system of differential Eqs. (55):

$$\mathbf{M}\ddot{\mathbf{q}} + \mathbf{\Phi}_{\mathbf{q}}^{\mathbf{T}}\lambda = \mathbf{Q} \tag{55}$$

Kinematic constraint Eq. (1)–(33) can be grouped into the following system of algebraic equations:

$$\mathbf{\Phi} = 0 \tag{56}$$

where $\mathbf{q}$ is the coordinate vector, $\mathbf{M}$ is the mass matrix of the system, $\mathbf{Q}$ is the vector of external forces, $\mathbf{\Phi_q}$ is the Jacobian matrix of the constraint equations and $\boldsymbol{\lambda}$ is the vector of the Lagrange multipliers.

The system of equations to be solved is given by expressions (55) and (56), which constitute a Differential-Algebraic system of Equations (DAE). To transform this DAE into a system of ODEs, the augmented Lagrangian method is used [18,26]:

As stated in [18], the augmented Lagrangian method leads to a simpler set of equations compared to a projection scheme method. Furthermore, the augmented Lagrangian formulation allows a straightforward calculation of the chain force. This force has to be obtained to guarantee that the upper section of the chain is always taut.

$$\left(\mathbf{M} + \alpha\mathbf{\Phi}_{\mathbf{q}}^{\mathrm{T}}\mathbf{\Phi}_{\mathbf{q}}\right)\ddot{\mathbf{q}} = \mathbf{Q} - \mathbf{\Phi}_{\mathbf{q}}^{\mathrm{T}}\left[\lambda_i + \alpha\left(\dot{\mathbf{\Phi}}_{\mathbf{q}}\dot{\mathbf{q}} + 2\xi\omega\dot{\mathbf{\Phi}} + \omega^2\mathbf{\Phi}\right)\right] \tag{57}$$

$$\lambda_{i+1} = \lambda_i + \alpha\left(\ddot{\mathbf{\Phi}} + 2\xi\omega\dot{\mathbf{\Phi}} + \omega^2\mathbf{\Phi}\right) \tag{58}$$

where the following parameters of the Baumgarte stabilization [27] are chosen:

$$\alpha = 10^5$$
$$\xi = 1$$
$$\omega = 10$$

The penalty parameter α takes a value of several orders of magnitude lower than if the penalty method were used. This is one of the advantages of the augmented Lagrangian formulation over the penalty method [18].

3.2. Integrator: Adams Bashforth Moulton + Trapezoidal

An Adams-Bashforth and Adams-Moulton solver was selected to solve this ODE system because of the stiffness of the problem. This stiffness is mainly due to the slip calculation, especially at the initial stages of the simulations, where sudden changes in the slip value were observed. Besides, sharp variations of F_z and F_x also occur when the wheels bounce and hit the ground.

Two types of integrators are used for the integration of the dynamic equations. The trapezoidal integrator is used to find the static equilibrium and the first four time steps of the simulation. The Adams-Bashforth and Adams-Moulton multi-step linear integrators are used for the rest of the simulation. The former is explicit and acts as a predictor, while the latter is implicit and acts as a corrector. This predictor-corrector strategy allows increasing the time steps and, consequently, accelerates the calculation process.

These mathematical tools have been developed to solve systems of first-order differential equations of the following form (59):

$$\dot{\mathbf{y}} = \mathbf{f}(\mathbf{y}, t) \tag{59}$$

Therefore, it is necessary to reduce the system of second order differential equations to a system of first order differential equations. To do so, the following transformations have been carried out:

$$\mathbf{y} = \begin{bmatrix} \mathbf{q} \\ \dot{\mathbf{q}} \end{bmatrix} \tag{60}$$

$$\dot{\mathbf{y}} = \begin{bmatrix} \dot{\mathbf{q}} \\ \ddot{\mathbf{q}} \end{bmatrix} \tag{61}$$

Once the transformations have been made, the trapezoidal integrator is used (62):

$$\mathbf{y}_{n+1} = \mathbf{y}_n + \frac{\Delta t}{2}(\dot{\mathbf{y}}_n + \dot{\mathbf{y}}_{n+1}) \tag{62}$$

While the Adams-Bashforth and Adams-Moulton integrators are defined by Eqs. (63) and (64) respectively:

$$\mathbf{p} = \mathbf{y}_{n+1} = \mathbf{y}_n + \frac{\Delta t}{24}(55\dot{\mathbf{y}}_n - 59\dot{\mathbf{y}}_{n-1} + 37\dot{\mathbf{y}}_{n-2} - 9\dot{\mathbf{y}}_{n-3}) \tag{63}$$

$$\mathbf{c}^* = \mathbf{y}_{n+1} = \mathbf{y}_n + \frac{\Delta t}{24}(9\dot{\mathbf{y}}_{n+1} + 19\dot{\mathbf{y}}_n - 5\dot{\mathbf{y}}_{n-1} + \dot{\mathbf{y}}_{n-2}) \tag{64}$$

Where **p** is the predictor (Adams-Bashforth) and **c*** is the corrector (Adams-Moulton). A parameter commonly used in CFD integrators, known as «under-relaxation factor» [28,29], has been used. This factor, ν, reduces integrator oscillations and improves method stability, especially with stiff problems. On the other hand, it reduces the convergence of the simulation. This parameter takes the value of 0.7 for all simulations in this work.

$$\mathbf{c} = \mathbf{y}_{n+1} = \begin{cases} \nu\mathbf{c}^* + (1-\nu)\mathbf{p} & \text{if } 1^{\text{st}} \text{ iteration} \\ \nu\mathbf{c}^*_{\text{new}} + (1-\nu)\mathbf{c}_{\text{old}} & \text{else} \end{cases} \tag{65}$$

This way, coordinate vector (**q**) is obtained from vector **c** (65). The error is calculated according to Eq. (66).

$$\text{error} = \sqrt{\sum \left(\mathbf{q}^{\text{new}}_{n+1} - \mathbf{q}^{\text{old}}_{n+1}\right)^2} \tag{66}$$

3.3. Initialization process: static equilibrium

The algorithm used to perform simulations is described below:

1. It starts by initializing the parameters of the simulation: time step, simulation time, geometry, suspension and tire parameters of the motorcycle.
2. A single-step trapezoidal solver is used to calculate the static equilibrium for the first time step.
3. The same single-step trapezoidal solver is used for the next four time steps.
4. During the rest of the simulation, the Adams Bashfort-Moulton's predictor-corrector multistep solver of the fourth order is used [30].

The static equilibrium position can be determined by means of different methods [18]. A trapezoidal solver from an approximate solution has been used in this work.

4. Optimization process

This Section describes the procedure followed in the optimization process by means of genetic algorithms. To perform this optimization, an objective function has to be defined. In this work, the objective function or fitness function takes into account the distance traveled by the motorcycle during 3.5 s of simulation and two penalties (67):

$$\text{Fitness Function} \equiv d \cdot \max\left\{\left(\frac{1}{\epsilon_1|SR - SR_{\text{optimum}}| + 1}\right) \cdot \left(\frac{1}{\epsilon_2|\text{slack}| + 1}\right); 0.95\right\} \tag{67}$$

The penalties are forced to be greater than 0.95. The nature of the penalties is described next. The first one, associated with the Squat Ratio (*SR*) [25], affects those solutions in which this parameter deviates from the optimum. According to [1,6,25,31], the optimal value of the SR should be close to 1. It is necessary to consider this phenomenon because an *SR* away from the unit causes the rear train to extend or to compress during an acceleration while exiting a curve, which is an unfavorable situation. This penalty prevents the swingarm from extending or compressing excessively when the motorcycle accelerates. The penalty factor ϵ_1 takes the value of 0.01.

The second parameter is associated with the length variation of the taut stretch of the chain throughout the simulation. This extension has to be guaranteed, so the lower stretch of the chain has to be left with the appropriate slack. Too much

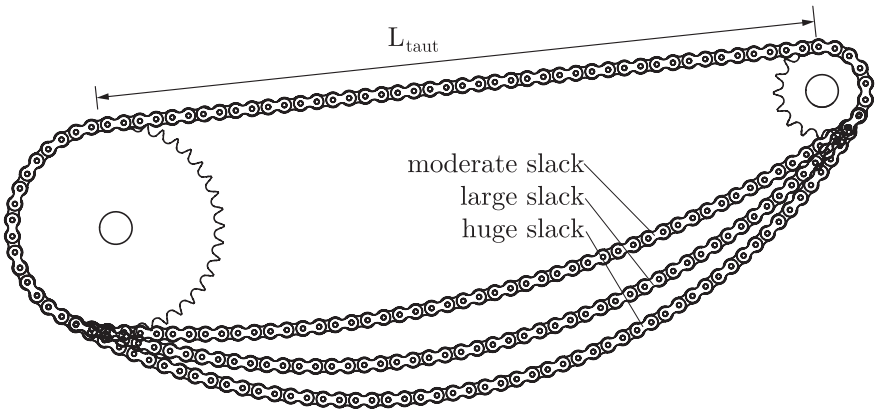

Fig. 6. Chain slack.

slack is not desirable, as it may even cause the chain to escape. The penalty factor ϵ_2 takes the value of $0.1\,\mathrm{m}^{-1}$. Slack is defined by expression (68):

$$\text{slack} = 2[\max(L_{\text{taut}}) - \min(L_{\text{taut}})]. \tag{68}$$

Therefore, the slack is the extra length that the loose part of the chain has in the most unfavorable situation (Fig. 6).

One of the reasons to carry out this work was to contribute to improving motorcycle models by taking into account the influence of swingarm movement in the slip of the rear wheel. Traction and braking control system performance is affected by the changes in the slip of the rear wheel. In this kind of system, the performance is commonly evaluated by minimizing the distance travelled by the motorcycle during the braking process or by maximizing the distance during the acceleration process. Thus, the distance travelled by the motorbike during a pre-determined period of time has been selected as the main factor in the fitness function.

Next, the optimization method used in this work is described. Among the different evolutionary optimization strategies, an algorithm known as differential evolution has been used. This method was described by Storn and Price in [32].

This algorithm has been used in a number of optimization problems applied to mechanical engineering, such as in the determination of the parameters of the Pacejka magic-formula [33] and in the synthesis of mechanisms [34]. The procedure can be summarized as follows (Fig. 7):

1. Initialization of the population through the generation of random individuals.
2. Evaluation of each individual and determination of the optimal one.
3. Generation of the new population through differential evolution:

$$\text{Parent}_2 = \text{Best Individual} + F \cdot (\text{Random Individual}_1 - \text{Random Individual}_2)$$

4. The new population is composed of a fraction of individuals from the previous generation. The remaining members of the new population come from the offspring of the differential evolution process.
5. From the new population, a fraction of individuals of the new population mutate.
6. The population resulting from this iteration is constituted by the best individuals from the population of parents and offspring. The best individual of this iteration is the best individual of the resulting population.
7. Steps 3 to 6 are repeated until the maximum number of iterations is reached.
8. The best individual of the last population is the solution to the optimization problem.

The lower and upper limits of the search space are listed in Table 8:

The rest of the design parameters (Table 4) as well as the suspension system parameters (Table 5) remain constant in all simulations, with the following exceptions:

Table 8
Search space. Genetic algorithm optimization.

Design Parameter	Description	Lower limit	Upper limit	Units
L_2	$\|\|\mathbf{r}_{1\to 2}\|\|$	0	0.2	m
a_2	$\measuredangle \mathbf{r}_{1\to 2}$	0	2π	rad
R_{WS}	Wheel sprocket radius	0.05	0.15	m

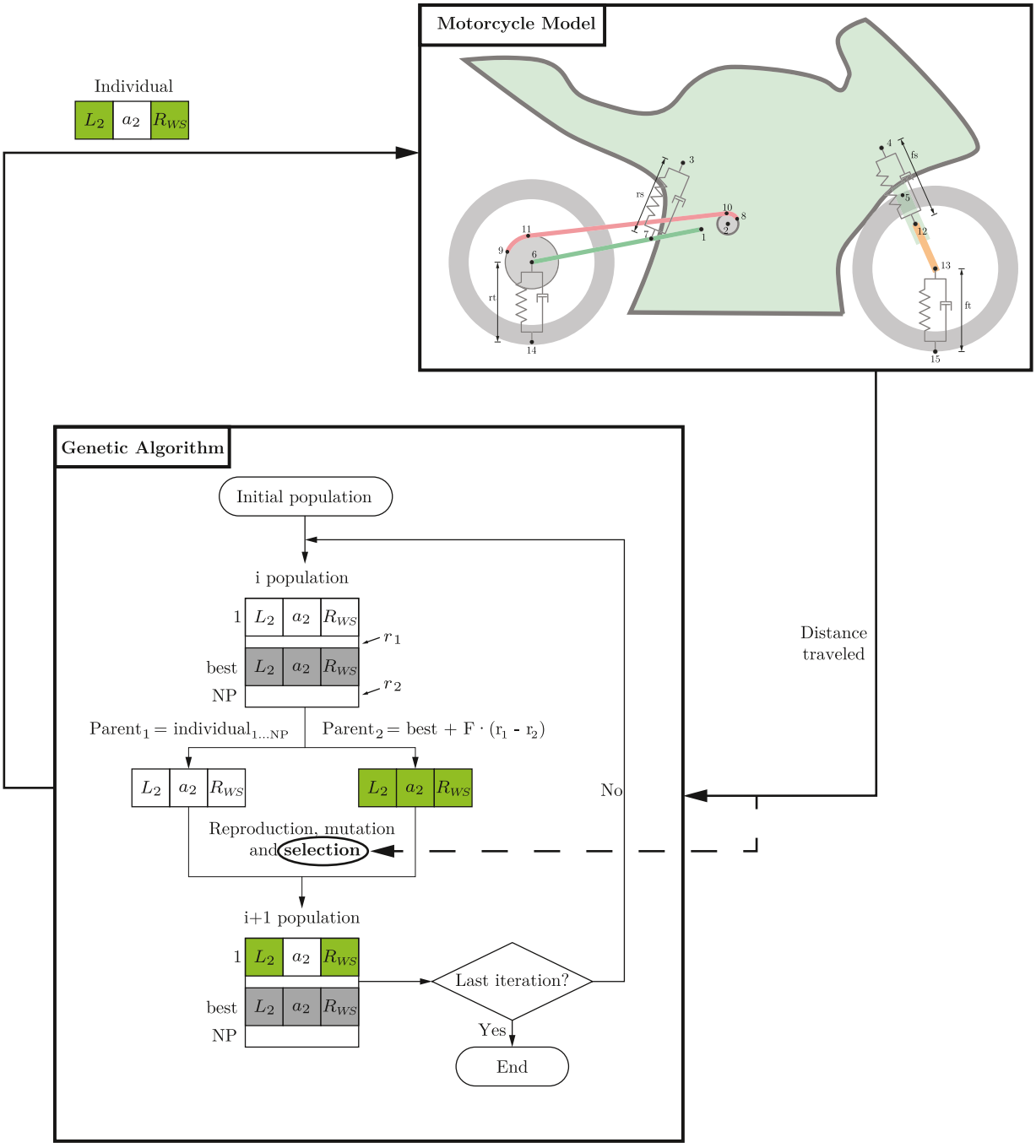

Fig. 7. Optimization algorithm.

- The ratio between the sprocket radii (R_{WS}/R_{ES}) is set at 2.0.
- The chain length is calculated from the geometry of the final drive (69), where subscript 0 indicates the first time step of the simulation.

$$L = (\gamma_0 - \alpha_0)R_{ES} + \sqrt{(x_{10,0} - x_{11,0})^2 + (y_{10,0} - y_{11,0})^2} + (\beta_0 - \gamma_0)R_{WS} \tag{69}$$

- The wavelength of the road, (λ), ranges from 2.0 to 5.0 m and the amplitude between 1 and 4 cm, in the case of the road with a sinusoidal profile.
- In the case of the road with a bump, the width, (σ), ranges from 0.2 to 1.0 m and the height between 2 and 4 cm.

Table 9
Search space. Sweep of variables .

Design Parameter	Description	Lower limit	Upper limit	Step size	Units
L_2	$\|\|\mathbf{r}_{1\to 2}\|\|$	0	0.2	0.02	m
a_2	$\measuredangle \mathbf{r}_{1\to 2}$	0	360	2	deg

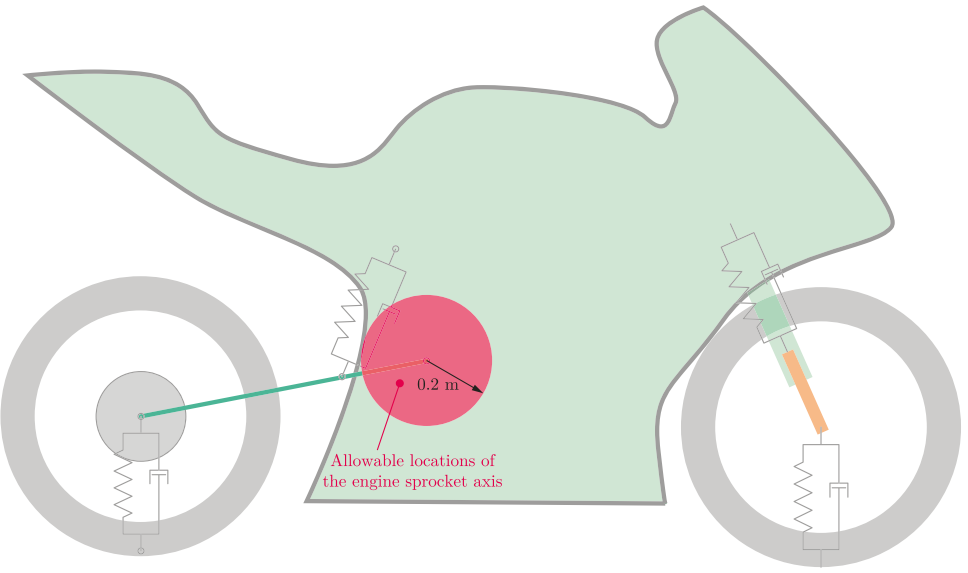

Fig. 8. Allowable locations of the center of the engine sprocket.

5. Results

The results of this study are grouped in two blocks. In the first block, a simulation has been carried out by sweeping parameters L_2 and a_2. In the second block, genetic algorithms have been used to optimize, in addition to the two parameters previously mentioned, the radius of the wheel sprocket (R_{WS}).

It is important to remark that a computational time ratio of 2.2 has been achieved. This is understood as the ratio between the simulation time and the time used for its calculation in a single core. Therefore, real time simulations have been achieved, with an average of 1.6 s to calculate 3.5 s of simulation in an Intel® Core™ i7-7700 CPU @ 3.60 GHz.

5.1. Case #1.- Sweep of variables

In this case, the variables are swept within the range set in Table 9 and Fig. 8:
The sweep has been made for a total of 23 different roads:

- Flat road.
- Sinusoidal road with four different wavelengths (2, 3, 4, and 5 m) and four amplitudes (1, 2, 3, and 4 cm).
- Gaussian (bumpy) road with three different widths (0.2, 0.5 and 1.0 m) and two heights (2 and 4 cm).

For each one of the 23 cases, the fitness function was evaluated by varying parameter a_2 in intervals of 2° from 0° to 360° and parameter L_2 in intervals of 0.02 m from 0 to 0.2 m. Therefore, a total of 45 540 simulations were carried out. The results are shown in Figs. 9–11.

5.2. Case #2.- Genetic algoritm optimization

In the case of the optimization using genetic algorithms, in addition to the two parameters indicated above (a_2 and L_2), the size of the wheel sprocket (R_{WS}) has also been optimized. As far as the road is concerned, the same 23 roads have been considered. The parameters that have been used for the genetic algorithm optimization are shown in Table 10.

The results are presented in Table 11, 12 and 13, which includes the optimal values of the design variables for all road types.

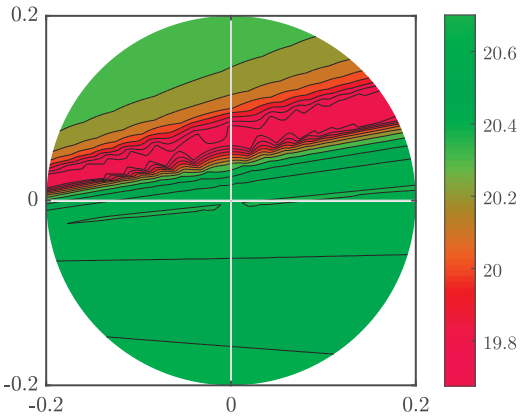

Fig. 9. Distance traveled by the motorcycle depending on the relative position of the engine sprocket axis with respect to the swingarm axis. Flat road.

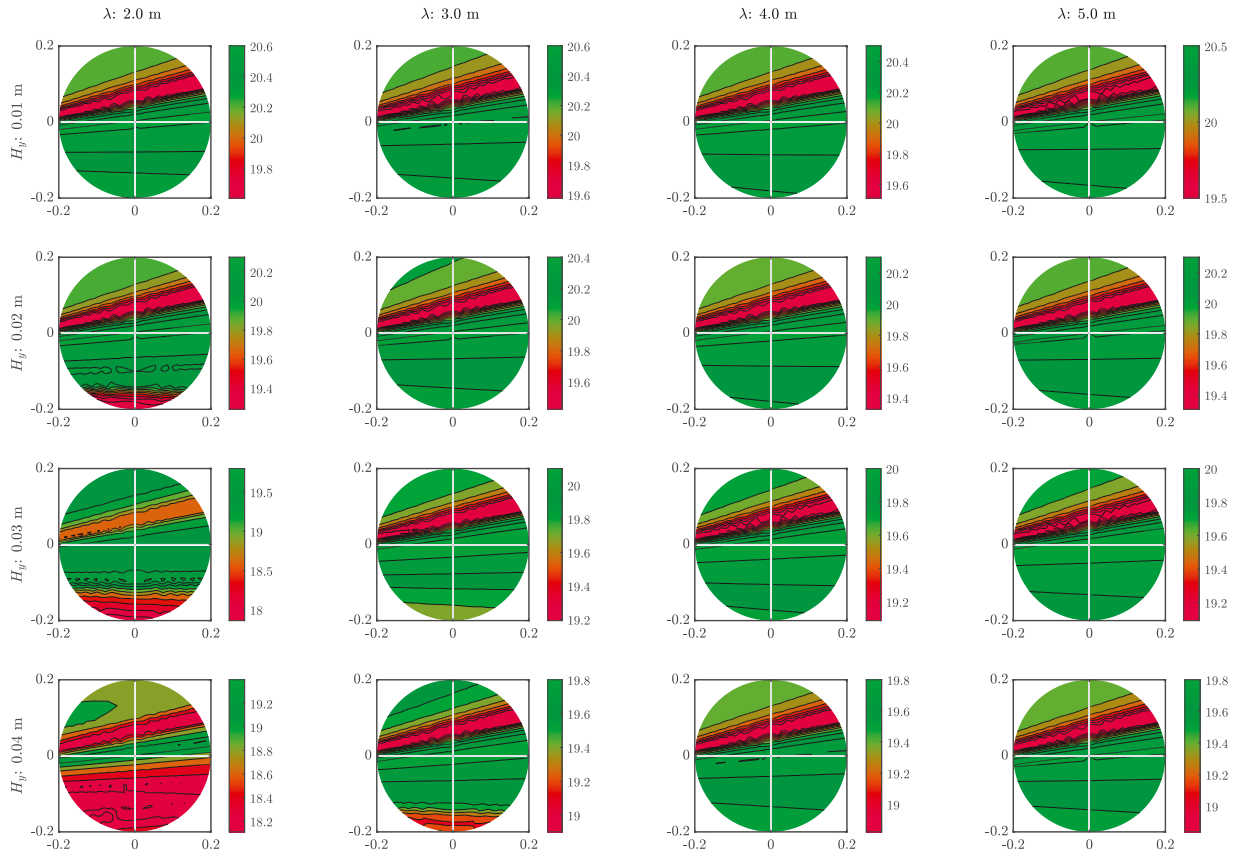

Fig. 10. Distance traveled by the motorcycle depending on the relative position of the engine sprocket axis with respect to the swingarm axis. Different wavelengths and heights of road.

Table 10
Genetic Algorithm optimization parameters.

Parameter	Description	Value
NP	Population size	50
F	Differential evolution F parameter	0.6
CP	Crossover probability	0.6
MP	Mutation probability	0.1
MR	Mutation range	0.2 · (Upper Limit - Lower Limit)
IterMax	Maximum number of iterations	50

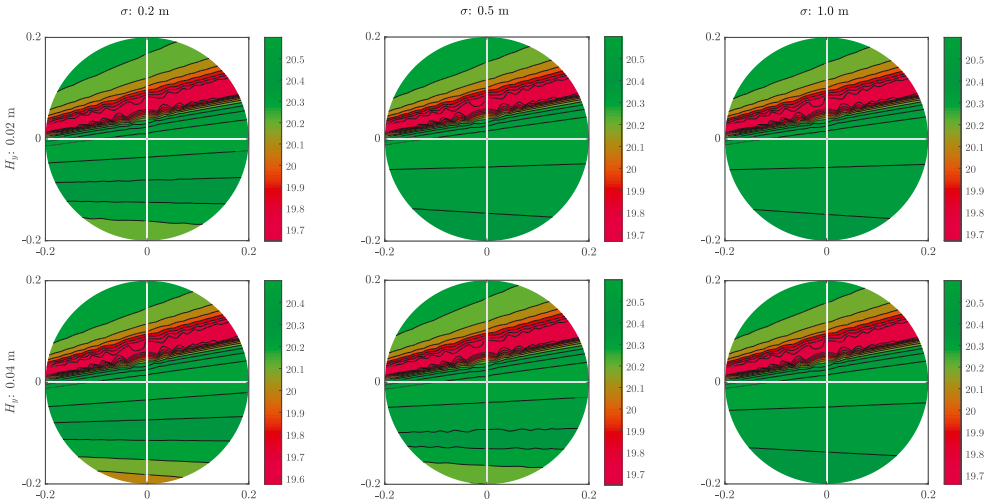

Fig. 11. Distance traveled by the motorcycle depending on the relative position of the engine sprocket axis with respect to the swingarm axis. Different bump sizes.

Table 11
Optimized parameters to maximize the fitness function. Road profile: Flat.

Best					
a_2	L_2	R_{WS}	Slack	SR	fitness fun
deg	m	m	mm	.	m
195.3	0.037	0.088	0.132	1.000	20.708

Table 12
Optimized parameters to maximize the fitness function. Road profile: Sinusoidal.

		Best					
H_y	λ	a_2	L_2	R_{WS}	Slack	SR	fitness fun
m	m	deg	m	m	mm	.	m
0.01	2.0	306.0	0.007	0.081	0.554	1.000	20.632
	3.0	263.0	0.009	0.115	0.532	1.000	20.604
	4.0	195.2	0.040	0.100	0.189	1.000	20.536
	5.0	211.7	0.017	0.106	0.354	1.000	20.520
0.02	2.0	199.8	0.027	0.091	0.553	1.000	20.329
	3.0	261.3	0.007	0.087	0.529	1.000	20.432
	4.0	325.5	0.011	0.092	0.606	1.000	20.338
	5.0	290.4	0.007	0.091	0.502	1.000	20.317
0.03	2.0	329.5	0.110	0.050	15.437	0.456	19.846
	3.0	296.6	0.005	0.062	0.742	1.000	20.184
	4.0	191.0	0.067	0.150	0.065	1.000	20.080
	5.0	191.3	0.063	0.121	0.046	1.000	20.092
0.04	2.0	371.0	0.200	0.050	0.503	1.397	19.410
	3.0	192.2	0.048	0.068	0.275	1.000	19.861
	4.0	294.5	0.006	0.074	0.698	1.000	19.804
	5.0	191.9	0.061	0.150	0.104	1.000	19.820

5.3. Discussion of results

From the results shown in Section 5.1, it can be seen that there are huge differences in the fitness function depending on the relative position of the engine sprocket axis with respect to the swingarm axis. The higher the road irregularities, the higher the difference in the results. In addition, the results of the optimizations lead to the following conclusion: the optimal position of the engine sprocket is aligned with the swingarm and very close to its axis (Fig. 12).

In this work, three parameters have been optimized: L_2, a_2 and R_{WS}. The swingarm length, (L_{SA}), and the swingarm design angle, (φ_0), have not been considered because they strongly affect the wheelbase and the equivalent stiffness of the rear suspension. This way, the optimization is not affected by the suspension system. Optimizing the value of the transmission

Table 13
Optimized parameters to maximize the fitness function. Road profile: Gaussian.

Best					
a_2	L_2	R_{WS}	Slack	SR	fitness fun
deg	m	m	mm	.	m
235.0	0.011	0.118	0.536	1.000	20.674
354.7	0.034	0.081	0.543	1.000	20.698
273.6	0.006	0.082	0.311	1.003	20.699
343.7	0.021	0.099	0.942	1.001	20.584
350.4	0.036	0.108	0.924	1.001	20.677
308.3	0.007	0.071	0.361	0.999	20.689

Table 14
Geometry parameters.

	Geometry 1	Geometry 2	Units
a_2	0	270	deg
L_2	0.00	0.15	m
R_{WS}	0.093	0.150	m
SR	1.092	0.239	–
Slack	0.000	67.270	mm
d	19.868	19.497	m

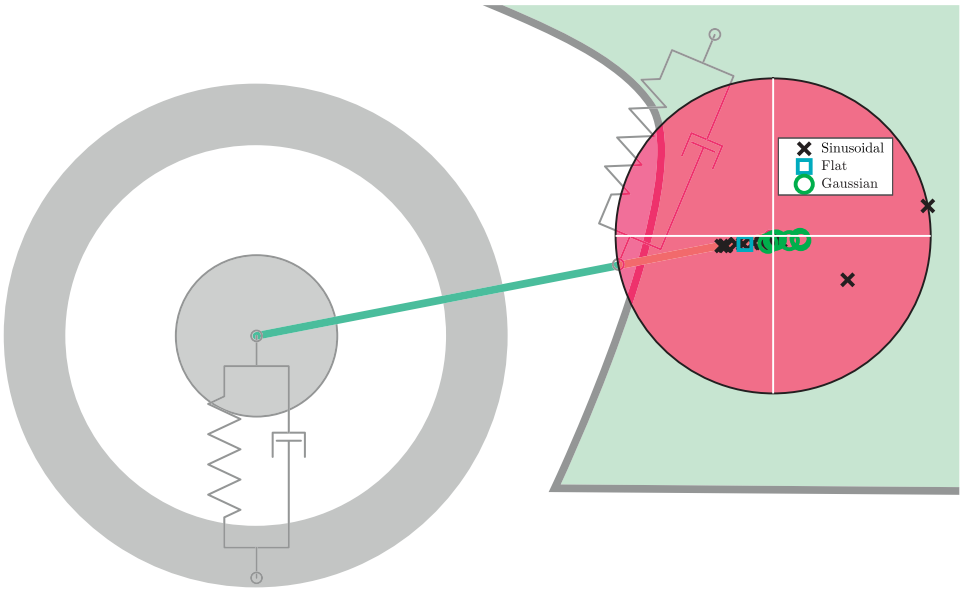

Fig. 12. Solutions from genetic algorithms.

ratio has not been considered either, since the objective is to determine the optimal position of the engine sprocket with respect to the swingarm axis.

On the other hand, it has been observed that it is necessary to model the entire motorcycle, allowing pitch and bounce vibration modes and not only the rear train. Previous simulations carried out with a simplified model showed that optimizations converged to a final drive geometry with the engine sprocket placed in the lowest positions if pitch and bounce movements were restricted. If the engine sprocket is placed very low, the force of the chain compresses the rear wheel. This increases its vertical load and reduces the effective radius, which maximizes the longitudinal force and, thus, the distance traveled. However, this simplification of studying only the rear axle is not valid since the load on the rear wheel cannot grow indefinitely. These phenomena have been eliminated by modeling the front train and allowing these two additional movements.

Fig. 13 shows the values of traveled distance, chain tension, squat ratio, vertical force, longitudinal slip and longitudinal force for the two geometries given in Table 14.

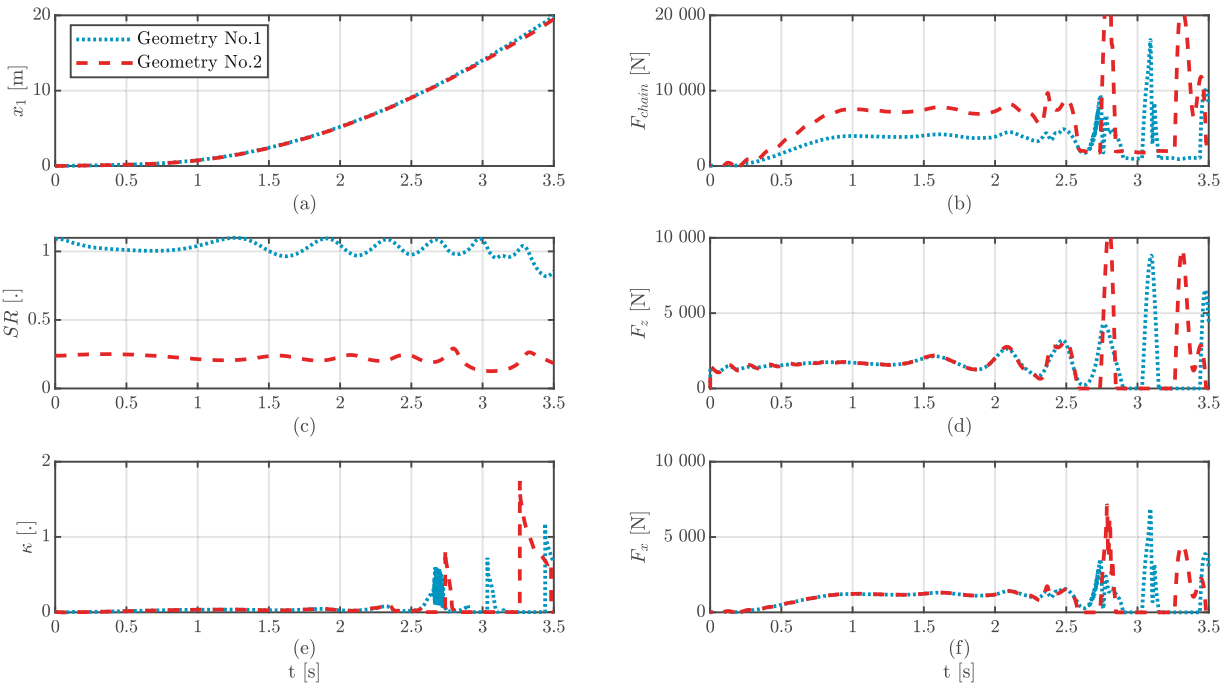

Fig. 13. Traveled distance, chain tension, squat ratio, vertical force, longitudinal slip and longitudinal force against time for two different geometries. Sinusoidal road: $H_y = 4$ cm, $\lambda = 3$ m.

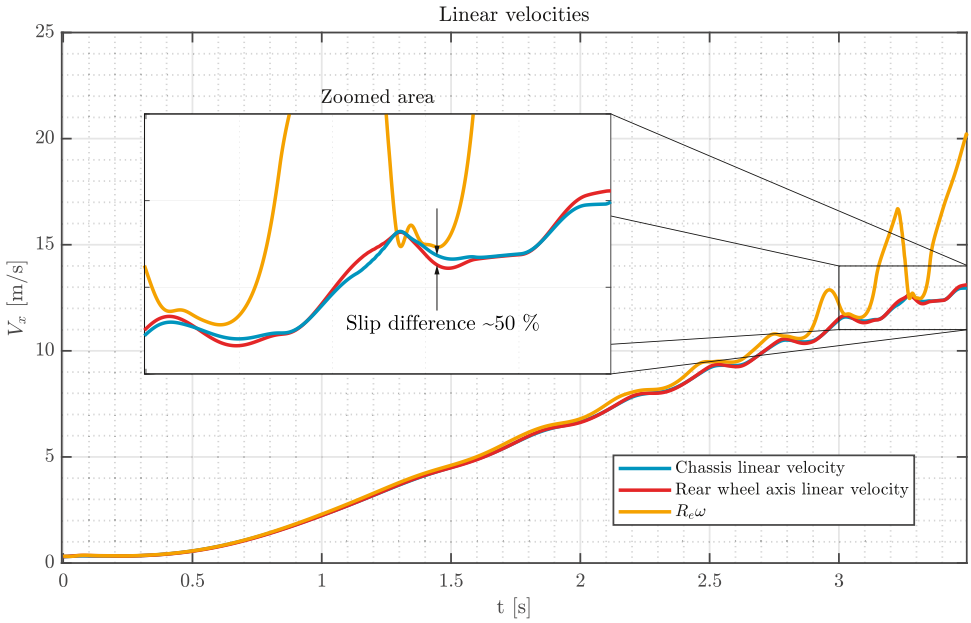

Fig. 14. Different linear velocities.

The first geometry (geometry 1) has been provided by the optimization algorithm. These results propose a configuration with concentric axes ($L_2 = 0$). The radius of the wheel sprocket is the average value provided by the 23 optimizations: $R_{WS} = 93$ mm.

For comparison purposes, a second geometry has been simulated. In this case, the sprocket is placed just below the swingarm axis at a distance of 150 mm, ($L_2 = 0.15$ m and $a_2 = 270^\circ$), and the radius of the wheel sprocket is 50 mm.

In this simulation, a sinusoidal road with an amplitude of 4 cm and a wavelength of 3.0 m was used. Differences up to 2% were observed in the distance traveled between both geometries (Fig. 13(a)). Fig. 13(e) also shows that the optimized

geometry leads to fewer slip fluctuations, which improves the stability of the motorcycle. Besides, the rear wheel of the optimized geometry stays in contact with the ground longer compared to the second geometry, which contributes to traveling a greater distance.

From the results shown in Fig. 13, it can be seen that it is necessary to consider a tire model that takes into account both the non-linearities that relate to the longitudinal slip and longitudinal force as well as the delay that exists in the generation of the longitudinal slip. This result implies that the interaction of the tire and the road with a simple tire model is not reproduced with sufficient accuracy for extreme conditions, such as the conditions analyzed in this paper, where sudden variations in vertical load and longitudinal slip occur.

It is also necessary to emphasize the importance of the proper selection of longitudinal velocity for the calculation of longitudinal slip (Eq. 39). Fig. 14 shows that the longitudinal slip velocity (V_{sx}), and therefore slip (κ), can be doubled depending on whether the linear velocity of the chassis or wheel axle is considered.

The video attached to this paper shows the simultaneous behavior of both configurations during 3.5 s of simulation, showing the results of this study.

6. Conclusions

In this work, an in-plane dynamic model of a motorcycle has been developed. Special attention has been given to the modeling of the transmission system and its influence on the power delivery.

A non-linear tire transient model has been used to reproduce the generation of contact forces between the tire and road. This model makes it possible to start the simulation from standstill, where slip calculation usually presents singularities and numerical errors. In addition, this model takes into account the delay that exists between the slip changes and the subsequent generation of contact forces. This characteristic of the proposed methodology is of particular interest in situations where sudden changes in the longitudinal slip take place, such as riding on irregular roads and during ABS and TCS operation.

The modeling of the motorcycle has been carried out by using 30 natural and 9 mixed coordinates respectively. This way, the mass matrix is constant and no Coriolis or centrifugal forces appear in the model equations. Consequently, a simplified formulation and easier programming of the dynamic equations are achieved.

An augmented Lagrangian formulation has been used. Implicit integrators have also been programmed, both single-step: trapezoidal, and multi-step: Adams-Bashforth (predictor) and Adams-Moulton (corrector). In addition, an under-relaxation factor has been employed to improve the stability of the integrator, which allows solving stiff problems. As a result, real time simulations have been achieved.

The model developed has been used to simulate the longitudinal dynamics of a motorcycle riding on uneven roads. In order to study the optimal configuration of the final drive elements, an optimization process of the relative position and size of the sprocket axis has been carried out. In this process,the transmission ratio is kept constant.

The results of this work show that, in order to maximize power transmission from the engine to the road, the optimal position of the engine sprocket axis relative to the swingarm axis should be virtually concentric or aligned with the swingarm. This conclusion is consistent with the usual configuration observed in sports motorcycles, in which power transmission has to be maximized.

Future works will include the optimization of the suspension system, including their non-linearities as well as the angle and length of the swingarm. Furthermore, the proposed model will be used to develop improved traction and braking control systems.

Declaration of Competing interest

The authors declare that they have no conflict of interest.

Acknowledgements

This work was partly supported by the Ministry of Economy, Industry and Competitiveness under grant TRA2015-67920-R, partly by the Ministry of Education, Culture and Sport under grant FPU17/03161.

Supplementary material

Supplementary material associated with this article can be found, in the online version, at doi:10.1016/j.mechmachtheory.2019.103647.

References

[1] V. Cossalter, R. Lot, M. Massaro, Modelling, Simulation and Control of Two-wheeled Vehicles, John Wiley & Sons Ltd, 2014, doi:10.1002/9781118536391.
[2] N. Srivastava, I. Haque, A review on belt and chain continuously variable transmissions (CVT): dynamics and control, Mech. Mach. Theory 44 (1) (2009) 19–41, doi:10.1016/j.mechmachtheory.2008.06.007.
[3] S. Burgess, C. Lodge, Optimisation of the chain drive system on sports motorcycles, Sports Eng. 7 (2) (2004) 65–73, doi:10.1007/bf02915918.

[4] V. Cossalter, R. Lot, M. Massaro, The chatter of racing motorcycles, Veh. Syst. Dyn. 46 (4) (2008) 339–353, doi:10.1080/00423110701416501.
[5] Y. Tezuka, Y. Shiomi, S. Kokubu, S. Kiyota, Vibration characteristics analysis in vehicle body vertical plane of motorcycle during turning, in: Annual Congress, JSAE Paper, 2004, pp. 219–224.
[6] R.S. Sharp, S. Evangelou, D.J.N. Limebeer, Multibody aspects of motorcycle modelling with special reference to autosim, in: J. Ambrósio (Ed.), Advances in Computational Multibody Systems, Springer Netherlands, 2005, pp. 45–68, doi:10.1007/1-4020-3393-1.
[7] M. Massaro, R. Lot, V. Cossalter, On engine-to-slip modelling for motorcycle traction control design, Proc. Inst. Mech.Eng. Part D 225 (1) (2011) 15–27, doi:10.1243/09544070JAUTO1575.
[8] R.S. Sharp, D.J. Limebeer, A motorcycle model for stability and control analysis, Multibody Syst. Dyn. 6 (2) (2001) 123–142, doi:10.1023/A:1017508214101.
[9] V. Cossalter, R. Lot, A motorcycle multi-body model for real time simulations based on the natural coordinates approach, Veh. Syst. Dyn. 37 (6) (2002) 423–447, doi:10.1076/vesd.37.6.423.3523.
[10] R.L. Jackson, I. Green, D.B. Marghitu, Predicting the coefficient of restitution of impacting elastic-perfectly plastic spheres, Nonlinear Dyn. 60 (3) (2010) 217–229, doi:10.1007/s11071-009-9591-z.
[11] M. Machado, P. Moreira, P. Flores, H.M. Lankarani, Compliant contact force models in multibody dynamics: evolution of the hertz contact theory, Mech. Mach. Theory 53 (2012) 99–121, doi:10.1016/j.mechmachtheory.2012.02.010.
[12] F. Marques, P. Flores, J.C. Pimenta Claro, H.M. Lankarani, A survey and comparison of several friction force models for dynamic analysis of multibody mechanical systems, Nonlinear Dyn. 86 (3) (2016) 1407–1443, doi:10.1007/s11071-016-2999-3.
[13] H.B. Pacejka, Tire and Vehicle Dynamics, 3, Elsevier, Oxford, 2012, doi:10.1016/C2010-0-68548-8.
[14] E. de Vries, H. Pacejka, Motorcycle tyre measurements and models, Veh. Syst. Dyn. 28 (1) (1998) 280–298, doi:10.1080/00423119708969565.
[15] D. Moreno Giner, Symbolic-Numeric Tools for the Analysis of Motorcycle Dynamics. Development of a Virtual Rider for Motorcycles based on Model Predictive, Universidad Miguel Hernández, 2016 Ph.D. thesis.
[16] A. Robison, A. Vacca, Multi-objective optimization of circular-toothed gerotors for kinematics and wear by genetic algorithm, Mech. Mach. Theory 128 (2018) 150–168, doi:10.1016/j.mechmachtheory.2018.05.011.
[17] F. Silva, M.A. Andrianoely, L. Manin, S. Ayasamy, C. Santini, E. Besnier, D. Remond, Optimization of power losses in poly-V belt transmissions via genetic algorithm and dynamic programming, Mech. Mach. Theory 128 (2018) 169–190, doi:10.1016/j.mechmachtheory.2018.05.016.
[18] J. Garcia de Jalon, E. Bayo, Kinematic and Dynamic Simulation of Multibody Systems, Springer New York, New York, 1994, doi:10.1007/978-1-4612-2600-0.
[19] L. Shampine, I. Gladwell, S. Thompson, Solving ODEs with MATLAB - Shampine Gladwell Thompson, Cambridge University Press, 1st edition.
[20] J.G. De Jalon, Twenty-five years of natural coordinates, Multibody Syst. Dyn. 18 (1) (2007) 15–33, doi:10.1007/s11044-007-9068-0.
[21] R.S. Sharp, S. Evangelou, D.J. Limebeer, Advances in the modelling of motorcycle dynamics, Multibody Syst. Dyn. 12 (3) (2004) 251–283, doi:10.1023/B:MUBO.0000049195.60868.a2.
[22] S. Mahalingam, Polygonal action in chain drives, J. Frankl. Inst. 265 (1) (1958) 23–28, doi:10.1016/0016-0032(58)90665-3.
[23] N. Fuglede, J.J. Thomsen, Kinematics of roller chain drives - Exact and approximate analysis, Mech. Mach. Theory 100 (2016) 17–32, doi:10.1016/j.mechmachtheory.2016.01.009.
[24] S. Evangelou, The Control and Stability analysis of Two Wheeled Road Vehicles, 2003 Ph.D. thesis.
[25] V. Cossalter, Motorcycle Dynamics, 2nd, LuLu, 2006, doi:10.1002/9781118536391.ch1.
[26] J. Nocedal, S. Wright, Numerical Optimization, 2nd, Springer, 2006.
[27] J. Baumgarte, Stabilization of constraints and integrals of motion in dynamical systems, Comput. Methods Appl. Mech.Eng. 1 (1) (1972) 1–16, doi:10.1016/0045-7825(72)90018-7.
[28] N. Fueyo, J.A. Blasco, Relaxation control in the solution of CFD problems, Int. J. Comput. Fluid Dyn. 13 (1) (1999) 43–63, doi:10.1080/10618569908940889.
[29] H. Versteeg, W. Malalasekera, An Introduction to Computational Fluid Dynamics, 2, Pearson Education, London, 2007.
[30] J. Cardenal, J. Cuadrado, P. Morer, E. Bayo, A multi-index variable time step method for the dynamic simulation of multibody systems, Int. J. Numer. Methods Eng. 44 (11) (1999) 1579–1598, doi:10.1002/(SICI)1097-0207(19990420)44:11<1579::AID-NME551>3.0.CO;2-5.
[31] T. Foale, Motorcycle Handing and Chassis Design the Art and Science, 1, 2002.
[32] K.S. Rainer, Prince, Differential evolution - a simple and efficient heuristic for global optimization over continuous spaces, J. Global Optim. 11 (1) (1997) 341–359, doi:10.1023/A:1008202821328.
[33] J. Cabrera, A. Ortiz, E. Carabias, A. Simon, An alternative method to determine the magic tyre model parameters using genetic algorithms, Veh. Syst. Dyn. 41 (2) (2004) 109–127, doi:10.1076/vesd.41.2.109.26496.
[34] J.A. Cabrera, A. Ortiz, F. Nadal, J.J. Castillo, An evolutionary algorithm for path synthesis of mechanisms, Mech. Mach. Theory 46 (2) (2011) 127–141, doi:10.1016/j.mechmachtheory.2010.10.003.